



## Article

# Research on the Production of Hydrogen Fluoride from Silicon Tetrafluoride Using 2.45 GHz Microwave Plasma

Songlin Liu <sup>1</sup>, Lianjun Shi <sup>1</sup>, Guilan Liu <sup>1,\*</sup>, Wei Xiao <sup>2,\*</sup>  and Huacheng Zhu <sup>3</sup> 

<sup>1</sup> The State Key Laboratory of Efficient Utilization for Low Grade Phosphate Rock and Its Associated Resources, Wengfu Group, Guiyang 550014, China; sll\_2024@163.com (S.L.); ljs\_2024@163.com (L.S.)

<sup>2</sup> College of Big Data and Information Engineering, Guizhou University, Guiyang 550025, China

<sup>3</sup> College of Electronics and Information Engineering, Sichuan University, Chengdu 610029, China; hczhu@scu.edu.cn

\* Correspondence: liuguilan8205@163.com (G.L.); wxiao@gzu.edu.cn (W.X.)

**Abstract:** Silicon tetrafluoride (SiF<sub>4</sub>), being a toxic gas, contains abundant fluorine and silicon resources. However, at present, the extraction of these resources from SiF<sub>4</sub> remains a significant challenge for current technologies. Microwave plasma emerges as a promising technology with considerable potential in this area. Nevertheless, the majority of research endeavors concentrate on the silicon production through microwave plasma treatment of SiF<sub>4</sub>, while the resultant tail gas, rich in fluorine resources, is neglected and subsequently wasted. In this paper, a low-pressure microwave plasma is employed to process SiF<sub>4</sub> and H<sub>2</sub> for the one-step synthesis of hydrogen fluoride (HF). The microwave power reflection ratio, electron density, SF<sub>4</sub> conversion rate, and produced HF concentration in varying microwave power levels and gas flow rates are obtained. The results demonstrate that all the processing parameters have a direct impact on the HF concentration. The maximum HF concentration of 11,200 ppm is achieved under the specific condition: an H<sub>2</sub> flow rate of 2.5 sccm, a SiF<sub>4</sub> flow rate of 2 sccm, and a microwave power level of 1100 W. Notably, this condition also results in the lowest energy cost. Moreover, the underlying reaction mechanism of the conversion from SiF<sub>4</sub> to HF is thoroughly analyzed. This work presents fundamental process guidance for the production of HF using microwave plasma, facilitating the scalability of this technology in industry.



Academic Editor: Nikolay Yu. Peskov

Received: 3 December 2024

Revised: 20 December 2024

Accepted: 22 December 2024

Published: 24 December 2024

**Citation:** Liu, S.; Shi, L.; Liu, G.; Xiao, W.; Zhu, H. Research on the Production of Hydrogen Fluoride from Silicon Tetrafluoride Using 2.45 GHz Microwave Plasma. *Processes* **2025**, *13*, 4. <https://doi.org/10.3390/pr13010004>

**Copyright:** © 2024 by the authors. Licensee MDPI, Basel, Switzerland. This article is an open access article distributed under the terms and conditions of the Creative Commons Attribution (CC BY) license (<https://creativecommons.org/licenses/by/4.0/>).

**Keywords:** microwave plasma; hydrogen fluoride production; silicon tetrafluoride treatment; low pressure

## 1. Introduction

The traditional process to prepare anhydrous hydrogen fluoride (AHF) is to react fluorite ore with sulfuric acid and then to purify the gaseous hydrogen fluoride by multiple distillation and re-crystallization [1]. This method is not only time-consuming and energy-intensive but also emits harmful gases, necessitating rigorous process management. Moreover, the raw material fluorite ore is a kind of scarce and nonrenewable mineral resource [2]. Hence, this traditional method of producing AHF from fluorite ore bears the problems of unsustainability and environmental concerns [3]. Recently, a novel mechanochemical method of generating HF from alkoxy-*gem*-difluorocyclopropane (gDFC) mechanophores is proposed [4]. The generated HF can be used in combination with fluoride indicators to generate an optical response and to degrade polybutadiene with embedded HF-cleavable silyl ethers. Nevertheless, the technical pathway of this method is complex, making it difficult to carry out large-scale application and promotion. Moreover, the HF can be generated from

the decomposition of the fluorochemicals, such as the conversion of alkali-metal-bound  $\text{CF}_3$  complexes [5] and hydrofluorocarbon [6–9], the thermal decomposition of the ammonium fluoride [10,11], and the discharge of the  $\text{SF}_6$  gas [12]. The raw materials required for the aforementioned processes of HF generation are challenging to obtain. During the recycling process of lithium-ion batteries, HF may also be generated [13–15]. However, the amount of HF generated during this process is very small, and it is harmful to the environment.

In the phosphate fertilizer industry, fluorosilicic acid is produced as a byproduct during the preparation of phosphoric acid from phosphorus ore [16]. This acid, abundant in fluorine and silicon resources, is often regarded as industrial waste from the phosphate fertilizer industry [17]. However, it can also serve as a crucial raw material for the production of AHF [18]. The methods of producing AHF from fluorosilicic acid can be divided into direct methods and indirect methods. The direct methods include the direct pyrolysis of fluorosilicic acid and the decomposition of fluorosilicic acid by concentrated sulfuric acid [19,20]. These methods face the challenges of high energy consumption, limited AHF purity, and emissions of the toxic gas silicon tetrafluoride ( $\text{SiF}_4$ ). The indirect methods involve utilizing fluorosilicic acid to react with a metal or metal oxide to yield fluorosilicate, followed by the application of the direct method to produce AHF from the resultant fluorosilicate [21–23]. The indirect methods can improve the purity of AHF, but the handling process is complicated, and they still bear the drawbacks of the direct methods.

During the process of preparing AHF from fluorosilicic acid, the toxic gaseous  $\text{SiF}_4$  is generated as a byproduct. Notably, this gas contains valuable fluorine and silicon resources that possess potential for recycling. This realization motivates us to explore the direct conversion of  $\text{SiF}_4$  into HF. As the fourth state of matter, the plasma is widely used in gas conversion applications, such as nitrogen fixation [24–26],  $\text{CO}_2$  conversion [27–29], and methane reforming [30–32]. The electron impact reactions within the plasma have the ability to transform gas molecules into atoms, ions, and radicals under gentle conditions (without the need for high temperatures or high pressures), thereby achieving the desired gas conversion. Due to this advantage, many scholars investigate the plasma treatment on  $\text{SiF}_4$ . For example, Vodopyanov A. V. and colleagues studied for the first time the decomposition of  $\text{SiF}_4$  in electron cyclotron resonance (ECR) microwave plasma for the purpose of depositing silicon [33]. They utilized the mass spectrometry method to measure the composition of the decomposition products of  $\text{SiF}_4$  as a function of various process parameters. Notably, they successfully obtained silicon films with excellent adhesion on both silicon and molybdenum wafers. Sennikov P. G. et al. used a radio-frequency (RF) discharge to convert  $\text{SiF}_4$  [34]. They achieved silicon deposition in an  $\text{H}_2/\text{SiF}_4$  plasma, with a maximum silicon yield of 60%, operated at a pressure of 0.2 Torr. Dornstetter J-C et al. also used RF plasma to grow silicon films from the dissociation of  $\text{SiF}_4/\text{H}_2/\text{Ar}$  gas mixtures [35]. By controlling the gas molar ratio, gas flow rate, and RF power, the amorphous silicon could transform into micro-crystalline silicon. Gaiaschi S. et al. conducted research on the deposition of hydrogenated micro-crystalline silicon–carbon alloy within a  $\text{SiF}_4/\text{CH}_4$  plasma that was generated by RF power [36]. Their findings revealed that the RF power density,  $\text{CH}_4$  flow rate, and the amount of  $\text{SiF}_4$  significantly influenced the micro structure of the resultant film. Kornev R. A. et al. developed a highly efficient inductively coupled plasma (ICP) method for obtaining silicon from  $\text{SiF}_4$  in the presence of argon [37]. This method achieved a silicon production rate of 0.9 g/h with an energy cost of 0.56 kWh/g.

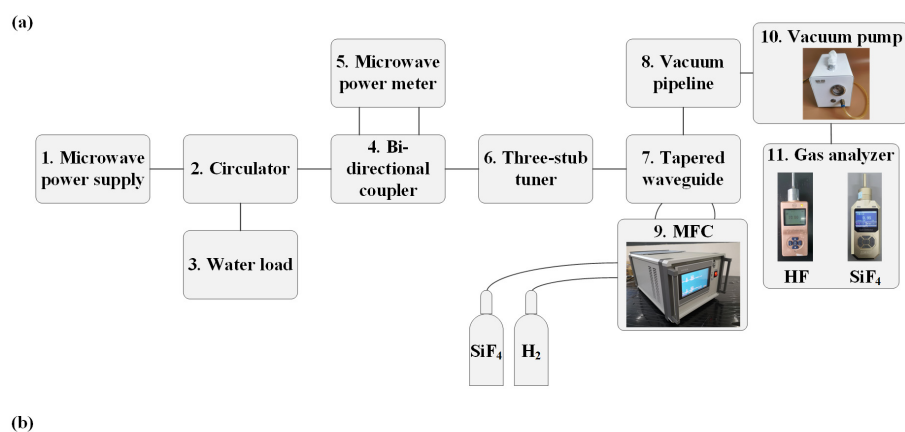
All the aforementioned investigations have exhibited that  $\text{SiF}_4$  can be dissociated within the plasma, ultimately yielding the valuable product silicon under appropriate process parameters. However, most of these investigations primarily focus on obtaining solid silicon from  $\text{SiF}_4$  using RF plasma, with a lack of reports detailing the conversion of  $\text{SiF}_4$  into HF. Therefore, this paper studies a one-step synthesis of HF using microwave

plasma technology, enabling instant control. And the underlying reaction mechanism of the conversion from  $\text{SiF}_4$  to HF is thoroughly analyzed. On the one hand, microwave plasma has the advantages of being electrodeless, possessing high electron density and electron energy, and having a longer lifespan compared to RF plasma. On the other hand, the HF product is valuable for industrial applications due to its expanding utilities across diverse sectors such as fluororubbers [38], pharmaceuticals [39], aerospace [40], semiconductors [41], fuels [42], and fluorocarbons [43].

## 2. Materials and Methods

### 2.1. Experimental Setup

A 2.45 GHz microwave plasma system based on the WR-430 waveguide was built for the HF production from  $\text{SiF}_4$  in this paper. The experimental system comprised four components: microwave transmission, gas intake, vacuum pumping, and gas composition measurement. Figure 1 shows the schematic and photograph of the system. The microwave was generated by a microwave power supply based on a magnetron (2M265, MUEGGE, Reichelsheim, Germany) cooled by water. The center frequency and maximum output power of the magnetron were 2.45 GHz and 3 kW, respectively. The circulator (MPWG22CIA01, Mapingtec, Chengdu, China) acted as the magnetron protection device, ensuring that the reflected power was absorbed by the water load (MPWG22WLA01, Mapingtec, Chengdu, China). The bi-directional coupler (MPWG22CPA01, Mapingtec, Chengdu, China) coupled the incident and reflected microwave power, which was then measured by the microwave power meter (KC9532, Measall Technology, Chengdu, China). The three-stub tuner (MPWG22THTA01P10KW, Mapingtec, Chengdu, China) was used to adjust the impedance match between the plasma and the WR-430 waveguide system. The electric field was concentrated within the tapered waveguide where the plasma was generated. The specific dimensions of this tapered waveguide have been detailed in our previous research [44].



(b)

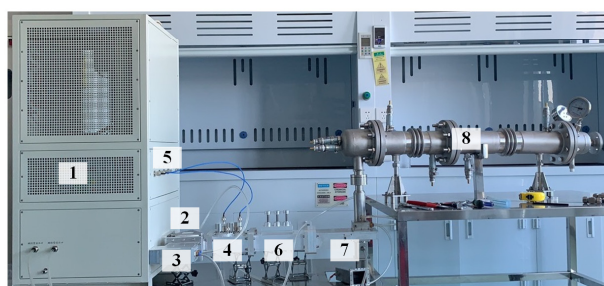


**Figure 1.** Microwave plasma experimental system for HF generation. (a) Schematic. (b) Photograph.

The working gas used in this paper consisted of SiF<sub>4</sub> and H<sub>2</sub>, both of which were stored in the gas cylinder and introduced into the discharge area of the tapered waveguide in a swirling motion. The gas flow rate was controlled by the mass flow controller (MFC, KT-C4Z, Ketanyiqi, Zhengzhou, China) with a range from 0 to 5 standard cubic centimeters per minute (sccm). Since the entire experiment needed to be conducted under a low pressure at about 0.7 atmospheres, a vacuum pump (FUJ-V3, Fujiwara, Taizhou, China) capable of achieving a vacuum up to 0.3 atmospheres was used and connected to the vacuum pipeline. The output gas was measured by two gas analyzers (PLT300-HF and PLT300-SiF<sub>4</sub>, Pultitong Electronics, Shenzhen, China) capable of detecting the HF concentration within a range of 0 to 20,000 parts per million (ppm) and the SiF<sub>4</sub> concentration within a range of 0 to 30,000 ppm. These two devices necessitated that the gas being measured be maintained at room temperature; hence, a vacuum pipeline equipped with water cooling was utilized to chill the output gas.

## 2.2. Electron Density Measurement

The electron density is one of the important indicators reflecting the activity of plasma. This parameter depends on the gas flow rate, gas composition, and microwave power. Therefore, this paper measured the electron density of the microwave plasma under different gas flow rates and microwave power levels. The measurement method in [44] was adopted to determine the electron density of the microwave plasma herein. The microwave power reflection ratio in the experiment was obtained initially, which was defined by the following formula:

$$\Gamma = \frac{P_{re}}{P_{in}} \times 100\% = 10^{-|S_{11}|/10} \quad (1)$$

where  $P_{re}$  and  $P_{in}$  represent the reflected and incident microwave power, respectively;  $S_{11}$  refers to the  $S$  parameter calculated by the simulation of the microwave-plasma interaction. The governing equation of this simulation is written as the Helmholtz equation,

$$\nabla \times \left( \frac{1}{\mu_r} \nabla \times \mathbf{E} \right) - \frac{\omega^2}{c_0^2} \varepsilon_p \mathbf{E} = 0 \quad (2)$$

where  $\mu_r$  indicates the permeability;  $\mathbf{E}$  denotes the electric field vector;  $\omega$  is the angular frequency of microwave;  $c_0$  is the light speed;  $\varepsilon_p$  refers to the relative complex permittivity of the plasma, which can be derived as the Appleton formula [45],

$$\varepsilon_p = 1 - \frac{\omega_p^2}{\omega_{co}^2} - j \frac{\omega_p^2 v_m}{\omega_{co}^2 \omega} \quad (3)$$

where  $\omega_p$  is the plasma angular frequency with  $\omega_p = [n_e \cdot e^2 / (\varepsilon_0 \cdot m_e)]^{1/2}$ , here  $n_e$  denotes the electron density, and  $m_e$  refers to the electron mass;  $v_m$  refers to the electron-neutral particle collision frequency;  $\omega_{co}$  represents the combination frequency, which can be derived as follows:

$$\omega_{co} = \sqrt{\omega^2 + v_m^2} \quad (4)$$

From the above equations, the electron density  $n_e$  determines the relative complex permittivity of the plasma. Here, a Gaussian model is assumed to describe the electron density distribution, which is written as

$$n_e = N_e \times \exp\left[-a_r \times \left(\frac{r-r_0}{R_p}\right)^2\right] \times \exp\left[-a(z) \times \left(\frac{z-h_0}{L_p}\right)^2\right] \quad (5)$$

where  $N_e$  indicates the maximum electron density number;  $a_r$  and  $a(z)$  are radial and axial fitting parameters, respectively, for adjusting the spatial electron density profile;  $r_0$  and  $h_0$  are the radial and axial coordinates of the plasma core in cylindrical coordinates, respectively;  $R_p$  is the radius of plasma, and  $L_p$  is the plasma length; The fitting parameter  $a(z)$  is a function of the  $z$ -axis written as

$$a(z) = \frac{1 - \text{sgn}(z - h_0)}{2} \cdot a_{z1} + \frac{1 + \text{sgn}(z - h_0)}{2} \cdot a_{z2} \quad (6)$$

where  $a_{z1}$  and  $a_{z2}$  are used to adjust the lower and upper axial electron density profile, respectively;  $\text{sgn}(x)$  represents the signum function.

Figure 2 shows the calculation domain of the microwave-plasma interaction. In Figure 2a, microwaves were incident from the left port of the waveguide (labeled as boundary AB in Figure 2c) and transmitted through the tapered waveguide into the quartz tube for the purpose of generating discharges. Two metal sleeves, EFLM and GHNO, were surrounding the quartz tube to prevent the microwave power leakage. Figure 2b shows a normalized electron density distribution derived from the above Gaussian model. The boundary conditions for both the waveguide wall and the metal sleeve wall were designated as perfect electric conductors (PECs), as specified by

$$\mathbf{n} \times \mathbf{E} = 0 \quad (7)$$

where  $\mathbf{n}$  is the unit normal vector perpendicular to the boundary. The top and bottom boundaries of the quartz tube IK and JP were assigned as the scattering boundary conditions (SBCs), as expressed in

$$\mathbf{n} \times (\nabla \times \mathbf{E}) - jk_0 \mathbf{n} \times (\mathbf{E} \times \mathbf{n}) = 0 \quad (8)$$

where  $k_0$  is the wave number in vacuum. The materials and boundary conditions for the pertinent domain are listed in Table 1.

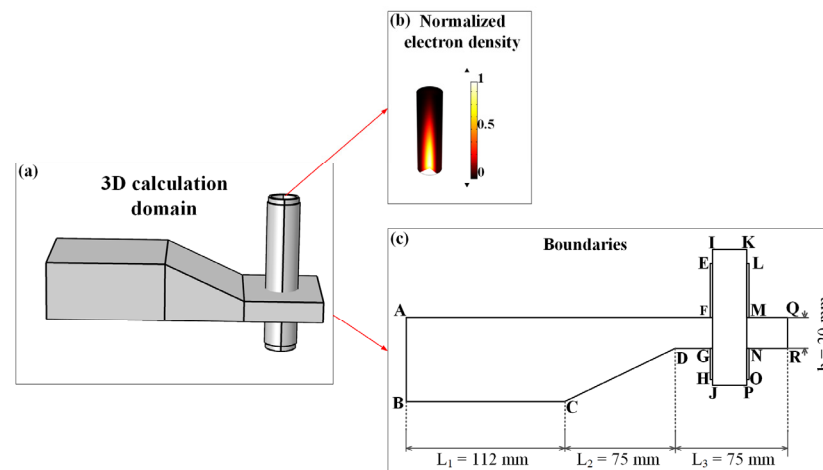


**Figure 2.** Schematic of (a) 3D domain of the microwave-plasma interaction, (b) electron density distribution model, and (c) boundaries.

**Table 1.** Properties of the calculation domain.

Object	Material	Boundary Condition
Waveguide	Aluminum	PEC: AF; BC; CD; DG; MQ; NR; QR.
Metal sleeve	Aluminum	PEC: EF; GH; LM; NO.
Quartz tube	Quartz	SBC: IK; JP

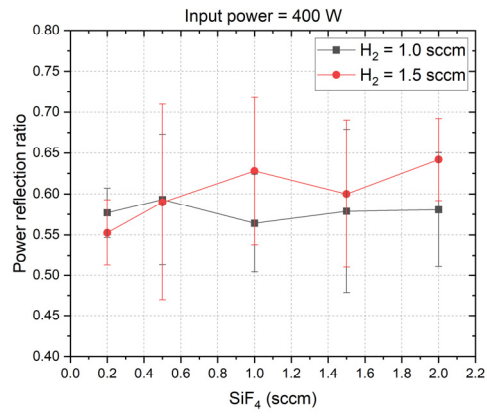
The commercial software COMSOL Multiphysics 5.5 was utilized to perform the microwave-plasma interaction simulation. Free tetrahedral meshes were generated for the calculation domain, resulting in a total of 683,846 meshes and 10,820,613 unknowns in the simulation. The computing platform was a workstation with the CPU of Intel (R) Core (TM) CPU i5-12400 @ 2.5 GHz and RAM of 128 GB based on the 64-bit Windows 10 operating system.

### 3. Results and Discussion

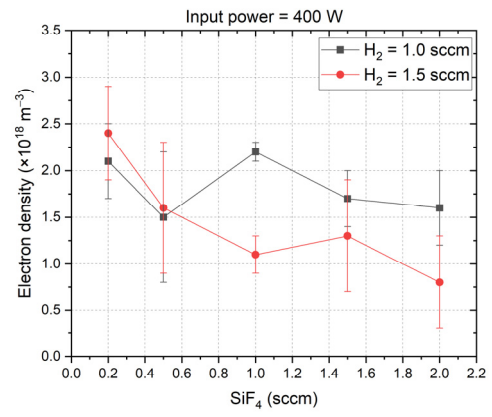
During the experimental process, the pressure in the discharge area was initially fixed at approximately 0.68 atmospheres using a vacuum pump prior to plasma ignition. Subsequently, H<sub>2</sub> was introduced into the quartz tube, and the microwave power supply was activated to excite the plasma. Once the plasma was ignited, SiF<sub>4</sub> was introduced into the quartz tube for conversion. The incident and reflected power values were recorded to calculate the power reflection ratio, which was then used to obtain the plasma electron density based on the method described in Section 2.2. Therewith, the output HF was measured at the outlet of the vacuum pump. In this work, the microwave power range varied from 400 W to 1100 W, and the flow rate of SiF<sub>4</sub> ranged from 0.2 sccm to 2 sccm. The H<sub>2</sub> flow rate varied at four levels: 1 sccm, 1.5 sccm, 2.0 sccm, and 2.5 sccm.

#### 3.1. Power Reflection Ratio and Electron Density

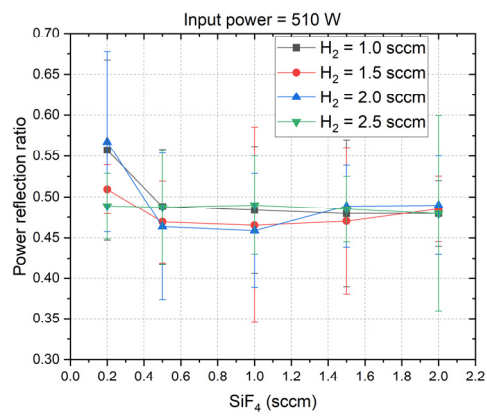
Figure 3 illustrates the microwave power reflection ratio and the corresponding electron density as they vary with the flow rates of SiF<sub>4</sub> and H<sub>2</sub>. At the microwave power of 400 W, the H<sub>2</sub> flow rate must not exceed 1.5 sccm in order to guarantee the ignition of plasma. At other microwave power levels, the H<sub>2</sub> flow rate can be set up to 2.5 sccm. There exists a notable negative correlation between the power reflection ratio and electron density when they are compared. That means a high power reflection ratio corresponds to a low electron density. The flow rates of SiF<sub>4</sub> and H<sub>2</sub> induce merely minor fluctuations in the power reflection ratio and electron density, and as the microwave power increases, these fluctuations progressively diminish. This is attributable to the fact that the plasma morphology and electron density remain relatively unaffected by the low gas flow rate in low-pressure environments [45]. At the microwave power level of 400 W, the power reflection ratio reaches its maximum value at about 0.6. The corresponding electron density is as low as about  $1.5 \times 10^{18} \text{ m}^{-3}$ . As the microwave power increases gradually to 1100 W, the power reflection ratio will decrease to around 0.2, and the electron density reaches up to  $11.5 \times 10^{18} \text{ m}^{-3}$ . These results indicate that increasing the microwave power can enhance the absorption of microwave power by the plasma, because the volume of the plasma is directly proportional to the microwave power it absorbs, meaning that a larger plasma volume results in higher microwave power absorption [44]. As the microwave power is increased from 400 W to 670 W, the power reflection ratio undergoes a notable decrement, dropping from 0.6 to approximately 0.2. Subsequently, further augmentation of the microwave power results in the power reflection ratio remaining virtually stable. This result demonstrates that as the microwave power rises to 670 W or higher, the dielectric properties of the plasma will become stabilized.



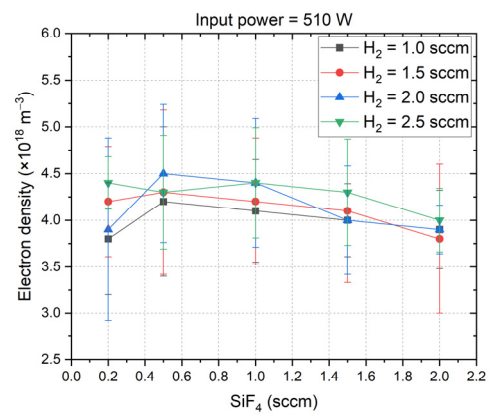
(a)



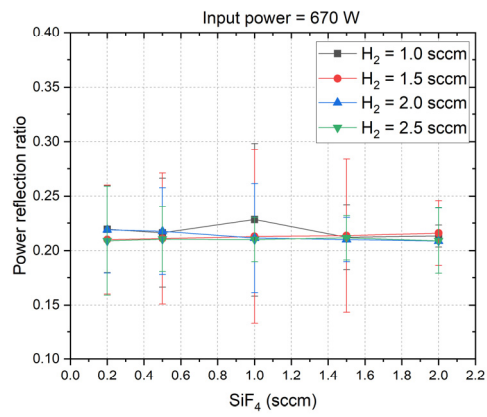
(b)



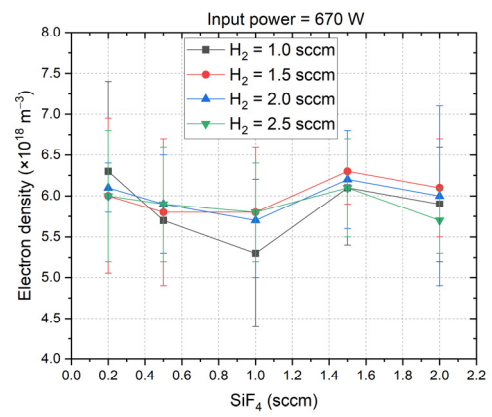
(c)



(d)



(e)



(f)

Figure 3. Cont.

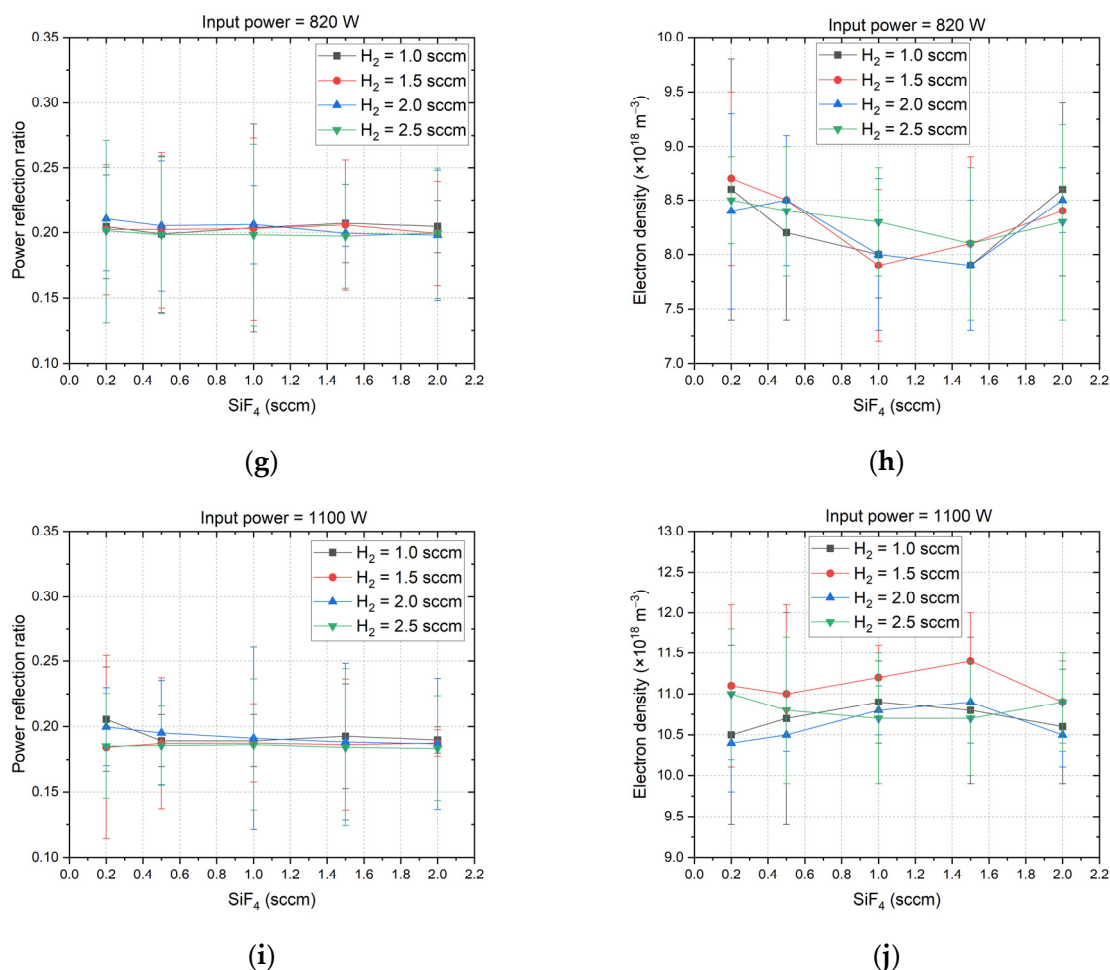


**Figure 3.** Microwave power reflection ratio and electron density under different microwave power levels. (a,b) 400 W; (c,d) 510 W; (e,f) 670 W; (g,h) 820 W; (i,j) 1100 W.

### 3.2. HF Production and SiF<sub>4</sub> Conversion

The measured HF concentrations of the output gases and the conversion rate of SiF<sub>4</sub> under different microwave power levels are shown in Figure 4. It is known that the concentration of the produced HF depends on the feeding gas flow rates and the microwave power. At 400 W, the HF concentration decreases with the SiF<sub>4</sub> flow rate but increases with the H<sub>2</sub> flow rate. Moreover, the decrement rate of HF concentration with the SiF<sub>4</sub> flow rate is larger when the H<sub>2</sub> flow rate is set to 1 sccm compared to when it is set to 1.5 sccm. Increasing the microwave power to either 510 W or 670 W does not change this trend; however, it results in a higher HF concentration and a smaller decrement rate. Additionally, the decrement rate of HF concentration remains nearly consistent across various H<sub>2</sub> flow rates. At a microwave power level of 820 W, the HF concentrations under different H<sub>2</sub> flow rates remain relatively stable with varying SiF<sub>4</sub> flow rates. As the microwave power increases to 1100 W, the HF concentrations across varying H<sub>2</sub> flow rates gradually increase with the SiF<sub>4</sub> flow rate, achieving a maximum concentration of approximately 11,200 ppm at an H<sub>2</sub> flow rate of 2.5 sccm and a SiF<sub>4</sub> flow rate of 2 sccm. The conversion rate of SiF<sub>4</sub> can be obtained by the following calculation:

$$\text{Conversion rate [\%]} = \left[ 1 - \frac{\text{Output SiF}_4 \text{ concentration [ppm]}}{\text{Input SiF}_4 \text{ concentration [ppm]}} \right] \times 100\% \quad (9)$$

where both the input and output SiF<sub>4</sub> concentrations are measured by the gas analyzer. It has been observed that increasing the microwave power enhances the conversion rate of



SiF<sub>4</sub>. Conversely, elevating the SiF<sub>4</sub> flow rate leads to a decrease in the conversion rate, as the increase in SiF<sub>4</sub> flow rate results in a higher input SiF<sub>4</sub> concentration.

It is reasonable that the increment in microwave power leads to an increment in HF concentration and SiF<sub>4</sub> conversion rate, because at a constant gas volume, an increment in the energy obtained per unit volume of the input gas leads to a more vigorous plasma impact reaction and a higher probability of SiF<sub>4</sub> and H<sub>2</sub> conversion to HF. This can be quantified by the specific energy input (SEI) written as

$$\text{SEI [kJ/mL]} = \frac{P [W] \times 10^{-3} [\text{kJ/J}] \times 60 [\text{s/min}]}{\text{Flow rate [sccm]}} \quad (10)$$

where  $P$  is the input microwave power.

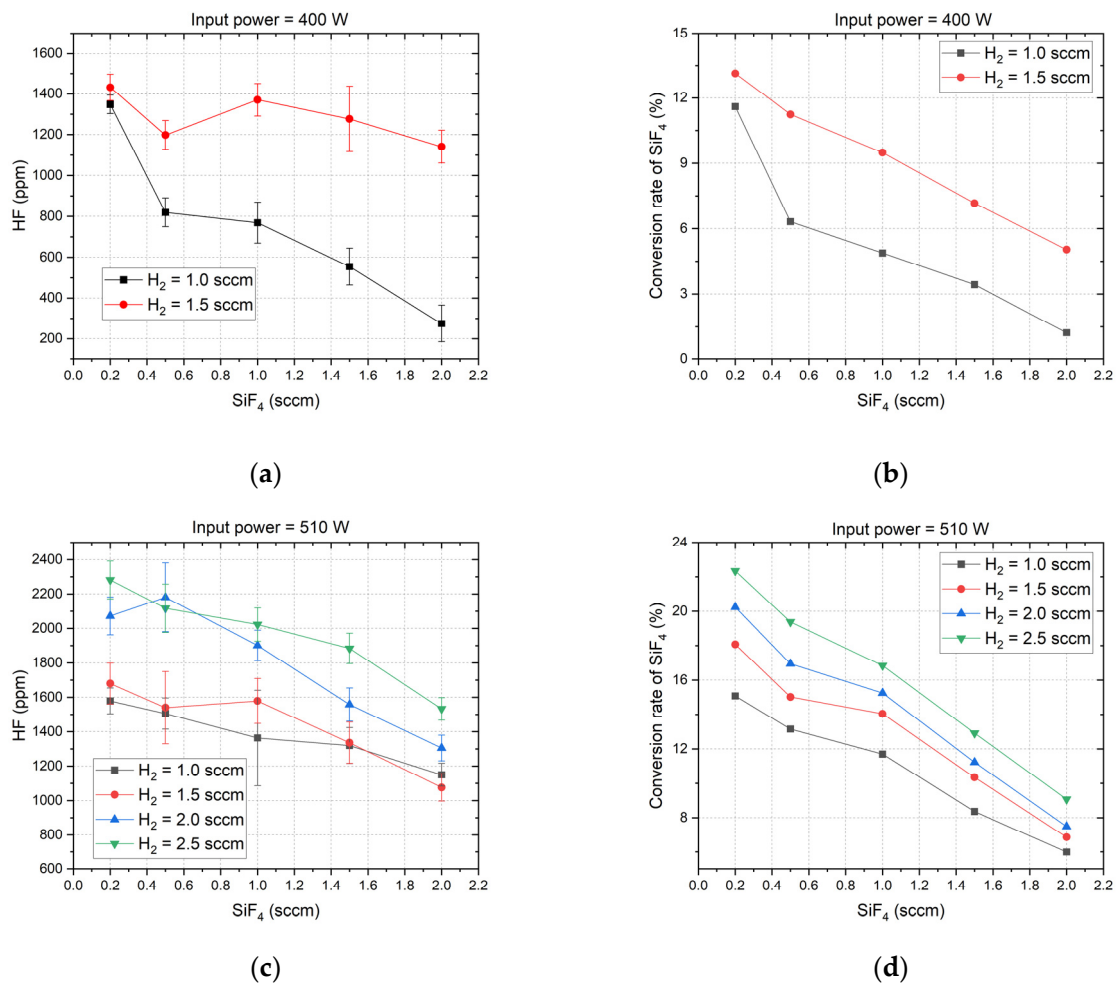
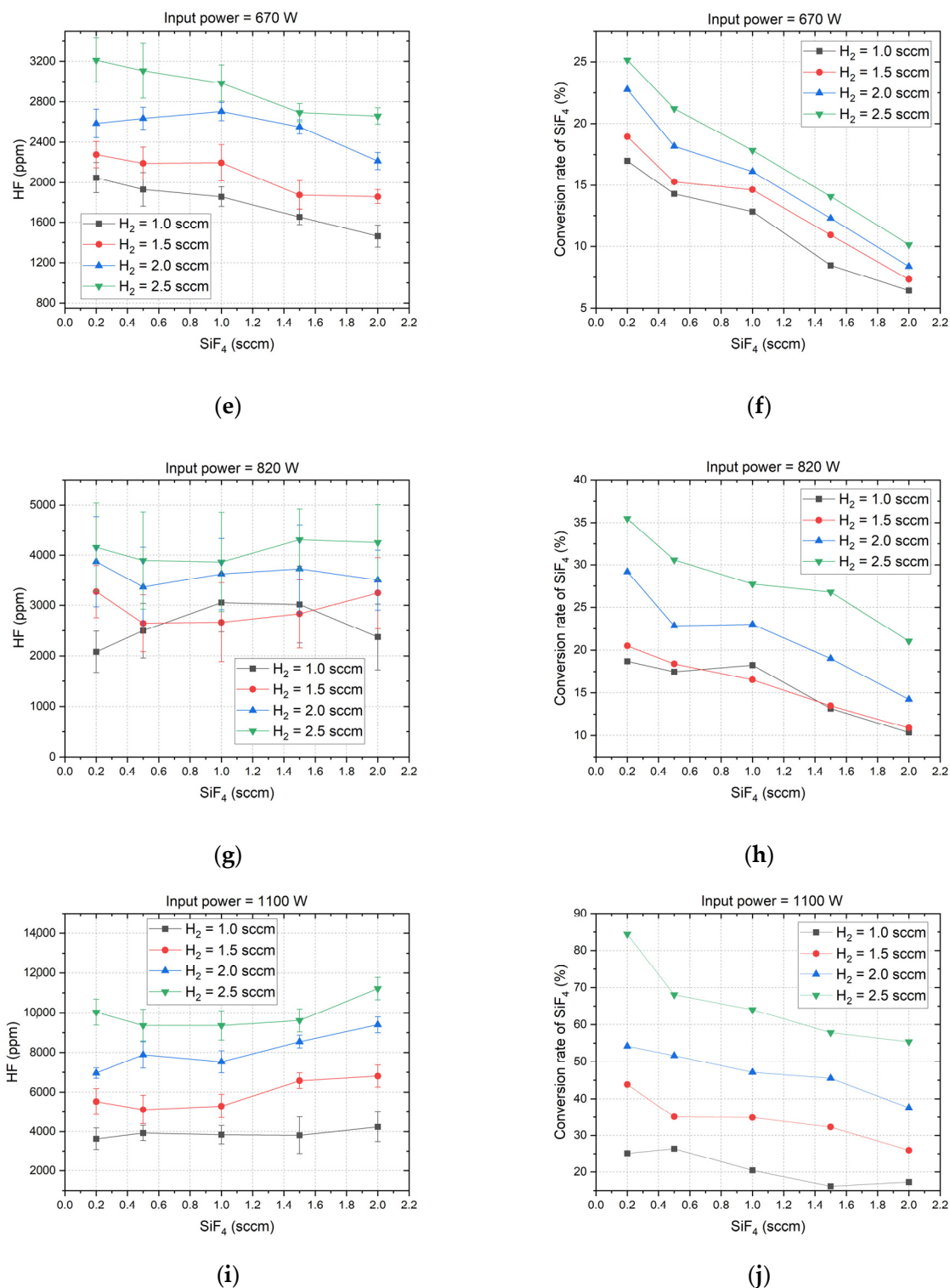
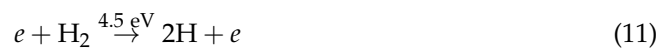


Figure 4. Cont.



**Figure 4.** HF production and conversion rate of SiF<sub>4</sub> under different microwave power levels. (a,b) 400 W; (c,d) 510 W; (e,f) 670 W; (g,h) 820 W; (i,j) 1100 W.

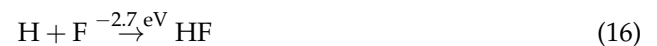
The key reaction pathway of the conversion process of SiF<sub>4</sub> and H<sub>2</sub> into HF is analyzed herein to facilitate a deeper understanding of the HF concentration curves presented in Figure 4. The dissociation of H<sub>2</sub> into H atoms within the plasma can be summarized in one reaction formula as:



where the dissociation energy is 4.5 eV. In the low-pressure plasma, this reaction can occur with a reduced energy of 3 eV [25]. The dissociation process of SiF<sub>4</sub> in the plasma is more complex than that of H<sub>2</sub>; its reaction formulas are shown as follows [46]:



Obviously, the dissociation of SiF<sub>4</sub> needs more energy compared to that of H<sub>2</sub>. The generated H atom and F atom can be combined to form HF molecules as [47]:



In the gas conversion process, H<sub>2</sub> is firstly dissociated in the plasma, followed by the dissociation of SiF<sub>4</sub>, because H<sub>2</sub> is initially introduced in the discharge area to form plasma. From Equations (11) to (16), we can deduce that, upon ignition of the H<sub>2</sub> plasma, almost all the H<sub>2</sub> molecules involved in the reaction can be dissociated into H atoms due to the low dissociation energy. Consequently, this results in the production of a greater number of H atoms compared to F atoms. In this case, if the microwave power remains at a low level and keeps constant, an increment in the SiF<sub>4</sub> flow rate will lead to a reduction in the SEI, which will impede the dissociation of a significant portion of SiF<sub>4</sub> into F atoms. Therefore, the produced HF concentration drops with the SiF<sub>4</sub> gas flow rate as illustrated in Figure 4a–e. When the microwave is at a high level, such as 820 W or 1100 W, the SEI is high enough to guarantee the dissociation of SiF<sub>4</sub> in high gas flow rates. As a result, increasing the SiF<sub>4</sub> flow rates can slightly increase the produced HF concentrations, as evidenced by the trends depicted in Figure 4g,i. Additionally, by increasing the microwave power, resulting in more high-energy electrons and a higher electron density, it is possible to intensify the dissociation of both H<sub>2</sub> and SiF<sub>4</sub>, ultimately facilitating the conversion of SiF<sub>4</sub> and the production of HF. This conclusion is supported by a comparison of the electron density results presented in Figure 3 with the results in Figure 4.

Based on the aforementioned reaction pathway, it is evident that the conversion process of SiF<sub>4</sub> yields byproducts such as SiF<sub>3</sub>, SiF<sub>2</sub>, SiF, and Si. However, it is important to note that SiF<sub>3</sub>, SiF<sub>2</sub>, and SiF are unstable at room temperature and prone to reacting with water in the air, leading to the formation of Si and HF. Consequently, these compounds must be stored under airtight and dry conditions to prevent such reactions. In contrast, Si remains in a solid state at room temperature and exhibits chemical inertness in the air. As mentioned in the Introduction, Si plays a crucial role as the fundamental material for the production of silicon-based semiconductors [33–37].

### 3.3. Energy Cost

The energy cost (EC) for producing HF by microwave plasma can be calculated by the following formula [48]

$$\text{EC [GJ/mol]} = \frac{\text{SEI [kJ/ml]} \times V_{\text{mol}} [\text{L/mol}] \times 10^3}{\text{HF [ppm]}} \quad (17)$$

where SEI is derived from Equation (9),  $V_{\text{mol}}$  represents the molar volume of ideal gas at room temperature and the pressure of 0.68 atmospheres with  $V_{\text{mol}} = 35.37 \text{ L/mol}$  [26]. Based on the measured results in Figure 4 and Equation (17), the EC under different

microwave power and gas flow rates is calculated as presented in Figure 5. Comparing Figure 5a through Figure 5e, it is observed that the EC decreases with the  $H_2$  flow rate. With the exception of the specific condition where the microwave power is set to 400 W and the  $H_2$  flow rate is maintained at 1 sccm, the EC will also drop down with the  $SiF_4$  flow rate. This is attributed to the low HF production in this condition. However, it is worth noting that the rate of decrement in EC with the  $SiF_4$  flow rate slows down when the  $H_2$  flow rate increases in different microwave power levels. Furthermore, when the  $H_2$  flow rate exceeds 1.5 sccm, an increment in microwave power can result in a decrement in EC, regardless of the  $SiF_4$  flow rate.

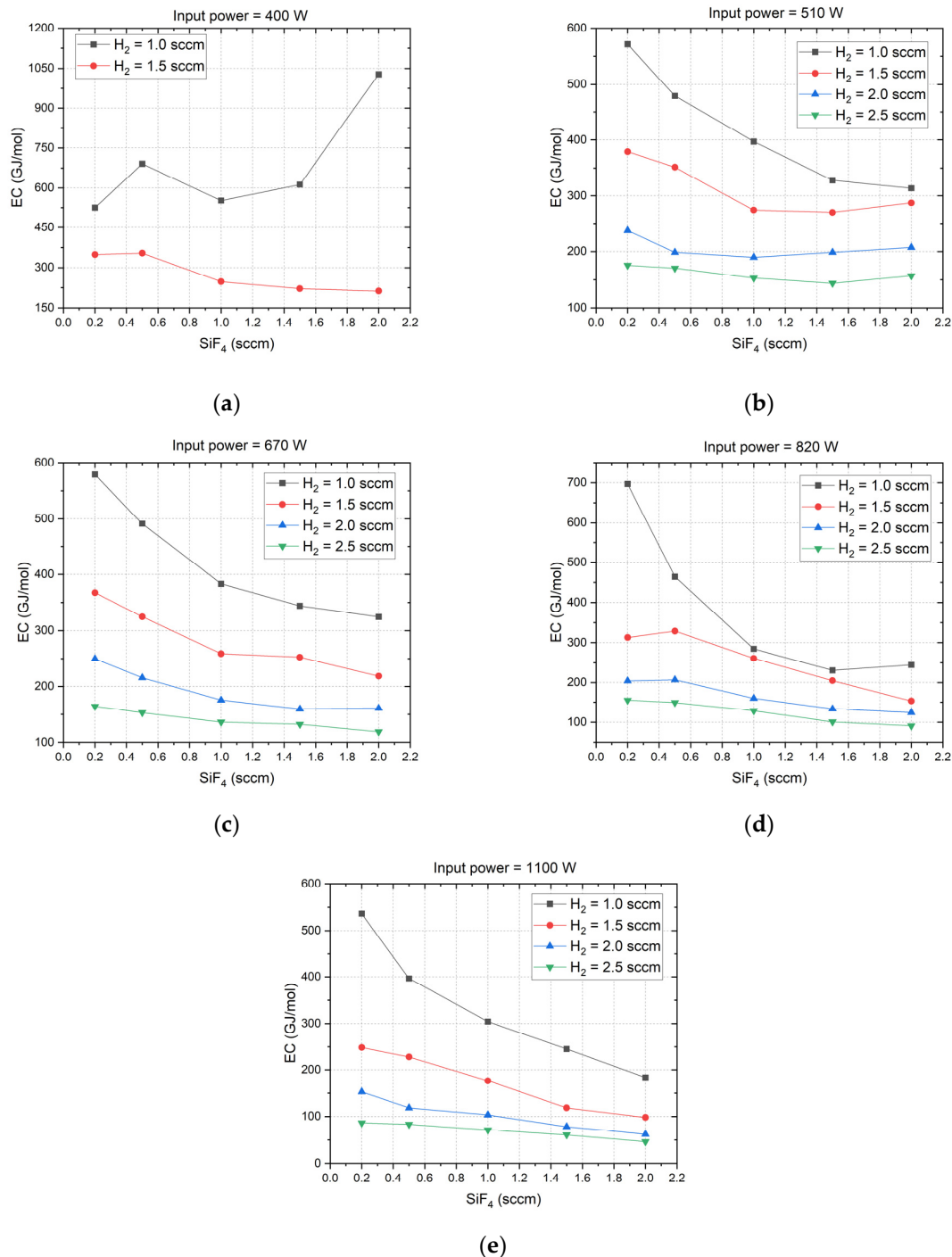


**Figure 5.** Energy cost for producing HF under different microwave power. (a) 400 W; (b) 510 W; (c) 670 W; (d) 820 W; (e) 1100 W.

The EC value for producing HF in this paper is three orders of magnitude (in units of GJ/mol) greater than that reported in other gas conversion applications utilizing plasma (in units of MJ/mol) [24–32]. This discrepancy arises because the gas flow rate employed here (in units of sccm) is three orders of magnitude lower than in those applications (in units of slm). Our future endeavor will be to enhance the gas processing capacity using low-pressure microwave plasmas. The lowest EC of 46.3 GJ/mol is attained with a microwave power setting of 1100 W and flow rates of 2.5 sccm for H<sub>2</sub> and 2 sccm for SiF<sub>4</sub>, respectively. This is also the condition of achieving the maximum HF concentration as depicted in Figure 4i.

### 3.4. Challenges of Scaling This Method in Industry

Although the proposed method in this paper can achieve the one-step synthesis of HF from SiF<sub>4</sub>, scaling this method from laboratory to industrial applications presents several hurdles. Notably, safety in production stands as a paramount concern. Given that H<sub>2</sub> is highly flammable and explosive, and SiF<sub>4</sub> is toxic, stringent measures must be taken to prevent any leakage of these gases throughout the process. Furthermore, the siting of production facilities must be meticulously considered. In particular, fiber Bragg grating (FBG) sensors, which have found extensive application in various gas detection scenarios, are anticipated to play a crucial role [49,50]. Their capacity to operate remotely [51] and in hyperbaric conditions [52] makes them especially suitable for this purpose. Additionally, the purification of the HF product causes another challenge. The tail gas resulting from our method contains not only HF but also impurities such as SiF<sub>4</sub>, H<sub>2</sub>, and other fluorine-containing gases, making the separation of HF from this mixture particularly difficult. One potential solution to this problem could lie in the use of specially prepared molecular sieves.

## 4. Conclusions

In this paper, a low-pressure microwave plasma was utilized to achieve a one-step synthesis of HF from the SiF<sub>4</sub> and H<sub>2</sub> mixtures. An experimental system was built up to study the process parameters influencing the HF production. In the experiments, the microwave power reflection ratio and electron density under different microwave power levels and SiF<sub>4</sub> and H<sub>2</sub> flow rates were acquired. The results revealed that as the microwave power level increased, the power reflection ratio decreased, whereas the electron density increased. The flow rates of SiF<sub>4</sub> and H<sub>2</sub> had merely minimal impact on both the power reflection ratio and electron density. The HF production was also measured in different process conditions. The results demonstrated that, on the one hand, the increment of the microwave power or H<sub>2</sub> flow rate could improve the produced HF concentration. On the other hand, at low microwave power levels ranging from 400 W to 700 W, the HF concentration decreased with the SiF<sub>4</sub> flow rate. Conversely, when the microwave power was above 800 W, the HF concentration slowly increased with the SiF<sub>4</sub> flow rate. The highest HF concentration achieved in this paper was 11,200 ppm, which was obtained at the microwave power of 1100 W and flow rates of 2.5 sccm for H<sub>2</sub> and 2 sccm for SiF<sub>4</sub>, respectively. Notably, the energy cost at this condition was also the lowest among all the process conditions, which was 46.3 GJ/mol. Moreover, the underlying reaction mechanism of the conversion from SiF<sub>4</sub> to HF is thoroughly analyzed. This work proposes an experimental investigation on the HF production by microwave plasma processing. However, the experimental parameters, particularly the SiF<sub>4</sub> and H<sub>2</sub> flow rates, are still at the laboratory scale. Further research is needed to enhance the gas processing capacity for the potential application of this method at an industrial scale.

**Author Contributions:** Conceptualization, S.L. and W.X.; methodology, G.L. and W.X.; software, H.Z.; validation, L.S. and W.X.; formal analysis, S.L.; investigation, G.L. and W.X.; resources, L.S.;

data curation, H.Z.; writing—original draft preparation, W.X.; writing—review and editing, S.L.; visualization, G.L.; supervision, S.L.; project administration, L.S.; funding acquisition, W.X. All authors have read and agreed to the published version of the manuscript.

**Funding:** This research was funded by the Postdoctoral project of the State Key Laboratory of Efficient Utilization for Low Grade Phosphate Rock and Its Associated Resources of Wengfu Group with grant number of YF(2023)018.

**Data Availability Statement:** The original contributions presented in this study are included in the article, further inquiries can be directed to the corresponding author.

**Conflicts of Interest:** The authors declare no conflicts of interest.

## References

1. Patel, C.; André-Joyaux, E.; Leitch, J.A.; De Irujo-Labalde, X.M.; Ibba, F.; Struijs, J.; Ellwanger, M.A.; Paton, R.; Browne, D.L.; Pupo, G.; et al. Fluorochemicals from fluorspar via a phosphate-enabled mechanochemical process that bypasses HF. *Science* **2023**, *381*, 302–306. [[CrossRef](#)] [[PubMed](#)]
2. Gao, Z.Y.; Wang, C.; Sun, W.; Gao, Y.S.; Kowalczyk, P.B. Froth flotation of fluorite: A review. *Adv. Colloid Interface Sci.* **2021**, *290*, 102382. [[CrossRef](#)]
3. Huang, J.W.; Zhang, Q.W.; Li, H.C.; Wang, C. Difficulties and recent achievements in flotation separation of fluorite from calcite—an overview. *Minerals* **2022**, *12*, 957. [[CrossRef](#)]
4. Hu, Y.X.; Wang, L.Q.; Kevlishvili, I.; Wang, S.; Chiou, C.Y.; Shieh, P.; Lin, Y.; Kulik, H.J.; Johnson, J.A.; Craig, S.L. Self-Amplified HF Release and Polymer Deconstruction Cascades Triggered by Mechanical Force. *J. Am. Chem. Soc.* **2024**, *146*, 10115–10123. [[CrossRef](#)]
5. Zhang, S.L.; Dong, J.J. Hydrogen-Bonding-Assisted  $\alpha$ -F Elimination from Cu-CF<sub>3</sub> for in Situ Generation of R<sub>3</sub>N·HF Reagents: Reaction Design and Applications. *Org. Lett.* **2019**, *21*, 6893–6896. [[CrossRef](#)]
6. Roh, S.A.; Kim, W.H.; Jung, D.S.; Hong, B.K. Thermal destruction of HFC-134a in pilot-, and full-scale gasification systems. *J. Energy Inst.* **2019**, *92*, 1842–1851. [[CrossRef](#)]
7. Krebs, R.; Owens, J.; Luckarift, H. Formation and detection of hydrogen fluoride gas during fire fighting scenarios. *Fire Saf. J.* **2022**, *127*, 103489. [[CrossRef](#)]
8. Yu, W.; Liu, C.; Li, Q.B.; Xin, L.Y.; Wang, S.K. Resource utilization of waste HFC-134a refrigerant by supercritical gasification method: A reactive molecular dynamic study. *Process Saf. Environ.* **2022**, *168*, 399–409. [[CrossRef](#)]
9. Kang, K.Y.; Kim, Y.J.; Kim, W.I.; Shin, S.K. Analytical method for combustible waste contaminated by the HF leakage from industrial process. *Anal. Sci. Technol.* **2014**, *27*, 167–171. [[CrossRef](#)]
10. Goma, I.; Mahmoud, M. Stimulating illitic sandstone reservoirs using in-situ generated HF with the aid of thermochemicals. *J. Pet. Sci. Eng.* **2020**, *190*, 107089. [[CrossRef](#)]
11. Hull, K.L.; Cairns, A.J.; Haq, M. Bromate Oxidation of Ammonium Salts: In Situ Acid Formation for Reservoir Stimulation. *Inorg. Chem.* **2019**, *58*, 3007–3017. [[CrossRef](#)]
12. Wan, J.J.; Zhao, X.H.; Li, K. Online Detection of Hydrogen Fluoride under Corona Discharge in Gas-Insulated Switchgear Based on Photoacoustic Spectroscopy. *Sensors* **2024**, *24*, 2806. [[CrossRef](#)] [[PubMed](#)]
13. Lux, S.F.; Chevalier, J.; Lucas, I.T.; Kostechi, R. HF Formation in LiPF<sub>6</sub>-Based Organic Carbonate Electrolytes. *ECS Electrochem. Lett.* **2012**, *2*, A121–A123. [[CrossRef](#)]
14. Chen, J.; Li, C.; Zhang, J.; Li, C.; Chen, J.; Ren, Y. First-Principles Study on the Adsorption and Dissociation of Impurities on Copper Current Collector in Electrolyte for Lithium-Ion Batteries. *Materials* **2018**, *11*, 1256. [[CrossRef](#)]
15. Rodrigues, M.T.F.; Liao, C.; Kalaga, K.; Shkrob, I.A.; Abraham, D.P. Dehydration Rather Than HF Capture Explains Performance Improvements of Li-Ion Cells by Ceramic Nanoparticles. *ACS Appl. Energy Mater.* **2019**, *2*, 5380–5385. [[CrossRef](#)]
16. Dahlke, T.; Ruffiner, O.; Cant, R. Production of HF from H<sub>2</sub>SiF<sub>6</sub>. *Procedia Eng.* **2016**, *138*, 231–239. [[CrossRef](#)]
17. Joshi, A.N. A review of processes for separation and utilization of fluorine from phosphoric acid and phosphate fertilizers. *Chem. Pap.* **2022**, *76*, 6033–6045. [[CrossRef](#)]
18. Yang, H.; Li, S.; Yu, H.; Liu, H.; Sun, K.; Chen, X. Production of anhydrous hydrogen fluoride from fluorosilicic acid: A review. *Front. Chem.* **2022**, *12*, 1372981. [[CrossRef](#)]
19. Reed, R.S. Production of High Purity Hydrogen Fluoride from Silicon Tetrafluoride. U.S. Patent 4,036,938, 19 July 1977.
20. AMani, K.; Chland, A.F. Process for the Recovery of Anhydrous Hydrogen Fluoride from Aqueous Solutions of Fluoro-Silicic Acid and Hydrogen Fluoride. U.S. Patent 4,389,293, 21 June 1983.
21. Hao, J. Study on producing anhydrous hydrogen fluoride by fluorosilicic acid and magnesium oxide and combined production of high quality magnesium sulfate. *Inorg. Chem. Ind.* **2019**, *51*, 40–43.

22. Zhao, C.; Xiao, F.; Wang, Z. Research progress in the preparation of hydrofluoric acid from fluorosilicic acid. *Organo-Fluor. Ind.* **2020**, *3*, 32–38.
23. Zhang, Y. Process technology and research progress of hydrofluoric acid production from by-product fluosilicic acid in phosphate rock processing. *Henan Chem. Ind.* **2023**, *40*, 12–15.
24. Patil, B.S.; Cherkasov, N.; Lang, J.; Ibhaddon, A.L.; Hessel, V.; Wang, Q. Low temperature plasma-catalytic NO<sub>x</sub> synthesis in a packed DBD reactor: Effect of support materials and supported active metal oxides. *Appl. Catal. B-Environ.* **2016**, *194*, 123–133. [[CrossRef](#)]
25. Pei, X.K.; Gidon, D.; Yang, Y.-J.; Xiong, Z.L.; Graves, D.B. Reducing energy cost of NO<sub>x</sub> production in air plasmas. *Chem. Eng. J.* **2019**, *362*, 217–228. [[CrossRef](#)]
26. Kelly, S.; Bogaerts, A. Nitrogen fixation in an electrode-free microwave plasma. *Joule* **2021**, *5*, 3006–3030. [[CrossRef](#)]
27. Snoeckx, R.; Bogaerts, A. Plasma technology—a novel solution for CO<sub>2</sub> conversion? *Chem. Soc. Rev.* **2017**, *46*, 5805–5863. [[CrossRef](#)] [[PubMed](#)]
28. Hecimovic, A.; D’Isa, F.A.; Carbone, E.; Fantz, U. Enhancement of CO<sub>2</sub> conversion in microwave plasmas using a nozzle in the effluent. *J. CO<sub>2</sub> Util.* **2022**, *57*, 101870. [[CrossRef](#)]
29. Wu, Y.; Li, S.Z.; Niu, Y.L.; Yan, H.J.; Yang, D.Z.; Zhang, J.L. Experimental investigation of CO<sub>2</sub> conversion in Boudouard reaction driven by an atmospheric-pressure microwave plasma torch. *J. Phys. D Appl. Phys.* **2023**, *56*, 065201. [[CrossRef](#)]
30. Liu, J.L.; Snoeckx, R.; Cha, M.S. Steam reforming of methane in a temperature-controlled dielectric barrier discharge reactor: The role of electron-induced chemistry versus thermochemistry. *J. Phys. D Appl. Phys.* **2018**, *51*, 385201. [[CrossRef](#)]
31. Tao, X.M.; Yang, C.; Huang, L.; Xu, D. DBD plasma combined with catalysts derived from NiMgAlCe hydrotalcite for CO<sub>2</sub> reforming of CH<sub>4</sub>. *Mater. Chem. Phys.* **2020**, *250*, 123118. [[CrossRef](#)]
32. Akande, O.; Lee, B. Plasma steam methane reforming (PSMR) using a microwave torch for commercial-scale distributed hydrogen production. *Int. J. Hydrogen Energy* **2022**, *47*, 2874–2884. [[CrossRef](#)]
33. Vodopyanov, A.V.; Golubev, S.V.; Mansfeld, D.A.; Sennikov, P.G.; Drozdov, Y.N. Experimental investigations of silicon tetrafluoride decomposition in ECR discharge plasma. *Rev. Sci. Instrum.* **2011**, *82*, 063503. [[CrossRef](#)]
34. Sennikov, P.G.; Golubev, S.V.; Kornev, R.A.; Mochalov, L.A.; Shilae, A.A. A Study of Silicon Tetrafluoride Reduction with Hydrogen in Radiofrequency Discharge. *High Energy Chem.* **2014**, *48*, 49–53. [[CrossRef](#)]
35. Dornstetter, J.-C.; Bruneau, B.; Bulkin, P.; Johnson, E.V.; Cabarrocas, P.R. Understanding the amorphous-to-microcrystalline silicon transition in SiF<sub>4</sub>/H<sub>2</sub>/Ar gas mixtures. *J. Chem. Phys.* **2014**, *140*, 234706. [[CrossRef](#)] [[PubMed](#)]
36. Gaiaschi, J.; Ruggeri, R.; Gueunier-Farret, M.-E.; Johnson, E.V. Use of radio frequency power, silicon tetrafluoride and methane as parameters to tune structural properties of hydrogenated microcrystalline silicon carbon alloys. *J. Phys. D Appl. Phys.* **2014**, *47*, 455102. [[CrossRef](#)]
37. Kornev, R.A.; Gornushkin, I.B.; Nazarov, V.V.; Shkrunin, V.E.; Ermakov, A.A. Features of hydrogen reduction of SiF<sub>4</sub> in ICP plasma. *Spectrochim. Acta B* **2022**, *195*, 106502. [[CrossRef](#)]
38. Manteau, B.; Pazenok, S.; Vors, J.-P.; Leroux, F.R. New trends in the chemistry of α-fluorinated ethers, thioethers, amines and phosphines. *J. Fluor. Chem.* **2010**, *131*, 140–158. [[CrossRef](#)]
39. Gardiner, J. Fluoropolymers: Origin, production, and industrial and commercial applications. *Aust. J. Chem.* **2015**, *68*, 13–22. [[CrossRef](#)]
40. Uhlenhake, K.E.; Yehia, O.R.; Noel, A.; Terry, B.C.; Örne, M.; Belal, H.M.; Gunduz, I.E.; Son, S.F. On the use of fluorine-containing nano-aluminum composite particles to tailor composite solid rocket propellants. *Propellants Explos. Pyrotech.* **2022**, *47*, e202100370. [[CrossRef](#)]
41. Steinert, M.; Acker, J.; Henbge, A.; Wetzig, K. Experimental studies on the mechanism of wet chemical etching of silicon in HF/HNO<sub>3</sub> mixtures. *J. Electrochem. Soc.* **2005**, *152*, C843. [[CrossRef](#)]
42. De Klerk, A.; De Vaal, P.L. Alkylate technology selection for Fischer-Tropsch syn crude refining. *Ind. Eng. Chem. Res.* **2008**, *47*, 6870–6877. [[CrossRef](#)]
43. Sicard, A.J.; Baker, R.T. Fluorocarbon refrigerants and their syntheses: Past to present. *Chem. Rev.* **2020**, *120*, 9164–9303. [[CrossRef](#)] [[PubMed](#)]
44. Xiao, W.; Liao, Y.H.; Wang, F.X.; Zhang, Z.P.; Zhu, H.C.; Yang, Y.; Huang, K.M. Determining Electron Density of Atmospheric Microwave Air Plasma Torch by Microwave Power Measurement. *IEEE Trans. Plasma. Sci.* **2022**, *50*, 1781–1789. [[CrossRef](#)]
45. Kim, J.H.; Kim, Y.C.; Chung, C.W. Experimental investigation on plasma parameter profiles on a wafer level with reactor gap lengths in an inductively coupled plasma. *Phys. Plasmas* **2015**, *22*, 073502. [[CrossRef](#)]
46. Mutsukura, N.; Ohuchi, M.; Satoh, S.; Machi, Y. The analyses of an SiF<sub>4</sub> plasma in an RF glow discharge for preparing fluorinated amorphous silicon thin films. *Thin Solid Films* **1983**, *109*, 47–57. [[CrossRef](#)]
47. Okada, Y.; Chen, J.; Campbell, I.H.; Fauchet, P.M.; Wagner, S. Mechanism of the growth of amorphous and microcrystalline silicon from silicon tetrafluoride and hydrogen. *J. Appl. Phys.* **1990**, *67*, 1757–1760. [[CrossRef](#)]

48. Wu, S.K.; Liao, Y.H.; Feng, K.; Zheng, F.; Xiao, W. Nitrogen fixation by atmospheric microwave plasma with local electric field enhancement. *J. Phys. D Appl. Phys.* **2025**, *58*, 015205. [[CrossRef](#)]
49. Zhou, X.; Dai, Y.T.; Karanja, J.M.; Liu, F.F.; Yang, M.Y. Microstructured FBG hydrogen sensor based on Pt-loaded WO<sub>3</sub>. *Opt. Express* **2017**, *25*, 8777–8786. [[CrossRef](#)] [[PubMed](#)]
50. Wang, C.Q.; Han, Z.W.; Wang, C.X.; Peng, G.D.; Rao, Y.J.; Gong, Y. Highly sensitive fiber grating hydrogen sensor based on hydrogen-doped Pt/WO<sub>3</sub>. *Sens. Actuat B-Chem.* **2024**, *404*, 135250. [[CrossRef](#)]
51. Kanwal, F.; Atieh, A.; Ghafoor, S.; Haq, A.; Qureshi, K.K.; Aziz, I.; Mirza, J. Remote monitoring of sleep disorder using FBG sensors and FSO transmission system enabled smart vest. *Eng. Res. Express* **2024**, *6*, 025337. [[CrossRef](#)]
52. Mirza, J.; Kanwal, F.; Salaria, U.A.; Ghafoor, S.; Aziz, I.; Atieh, A.; Almogren, A.; Haq, A.U.; Kanwal, B. Underwater temperature and pressure monitoring for deep-sea SCUBA divers using optical techniques. *Front. Phys.* **2024**, *12*, 1417293. [[CrossRef](#)]

**Disclaimer/Publisher’s Note:** The statements, opinions and data contained in all publications are solely those of the individual author(s) and contributor(s) and not of MDPI and/or the editor(s). MDPI and/or the editor(s) disclaim responsibility for any injury to people or property resulting from any ideas, methods, instructions or products referred to in the content.